Journal of Sol-Gel Science and Technology (2022) 102:466–477
https://doi.org/10.1007/s10971-022-05771-7

INVITED PAPER: FUNCTIONAL COATINGS, THIN FILMS AND MEMBRANES (INCLUDING DEPOSITION TECHNIQUES)

Bioinspired silica-based sol–gel micropatterns on aluminium for humid air condensation

Maria Basso[1] · Elena Colusso[1] · Alessandro Sacco[1] · Marco Tancon[1] · Stefano Bortolin[1] · Matteo Mirafiori[1] · Massimo Guglielmi[1] · Alessandro Martucci[1]

Received: 30 September 2021 / Accepted: 6 March 2022 / Published online: 1 April 2022

Abstract

Several patterned coatings with a hybrid organic-inorganic nature were deposited on metallic substrates by exploiting the dewetting of a sol–gel bilayer. The hybrid coatings, inspired by the exoskeleton of a desert beetle, consisted of hydrophilic silica droplets on a hydrophobic CH_3-silica bottom layer. The patterned morphology was tuned by changing the initial solution concentration, which resulted in substantial changes in the size and the density of distribution of the hydrophilic droplets. The reproducibility of the dewetting process on metallic substrates was confirmed, together with its scalability over large area substrates. The real-life application of the patterned coating for atmospheric water harvesting was tested in a custom-made apparatus, which demonstrated that the patterned coating led to a higher collected mass during condensation from humid air compared to the bare aluminium substrate. The patterned coating was proven to maintain its structure after the humid air exposure, confirming the robustness of the sol–gel-based materials.

Graphical abstract

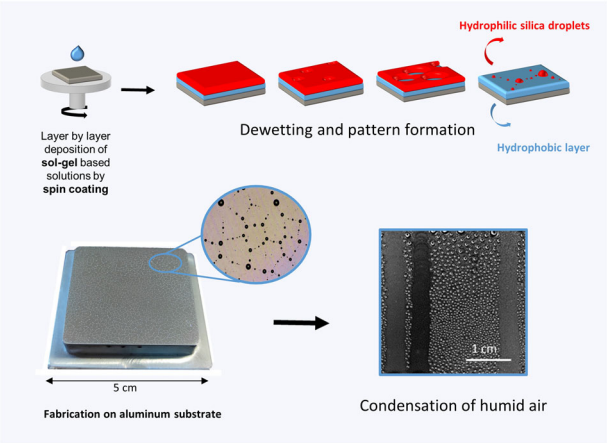

Keywords Micropattern · Hybrid sol–gel film · Dewetting · Humid air condensation · Wettability · Metallic substrate

Supplementary information The online version contains supplementary material available at https://doi.org/10.1007/s10971-022-05771-7.

✉ Alessandro Martucci
alex.martucci@unipd.it

[1] Università di Padova, Dipartimento di Ingegneria Industriale, Padova, Italy

Highlights

- Fabrication of hydrophilic-hydrophobic sol–gel patterns on metallic substrates.
- Environmental stability of patterned coating in conditions of high relative humidity demonstrated.
- Improved condensed mass during humid air condensation of patterned coating with respect to uncoated aluminium sample.

1 Introduction

The global drinkable water scarcity emphasises the need to find alternative paths to sustain the increasing water demand. As reported in the FAO 2020 publication, today 1.2 billion people, almost one-sixth of the world's entire population, live in agricultural areas which suffer from severe water scarcity [1]. Urgent solutions are required to solve this problem and several hypotheses have been proposed in recent years, from solar-driven desalination plants [2] to membrane-based distillation systems for contaminated water [3]. Among the various approaches, a promising solution to replenish our water supplies is given by the collection of water from the vapour present in humid air. Water condensation on a surface is subjected to nucleation and growth phenomena, which are influenced by the wettability of the surface. By acting on the latter, it is possible to favour specific dynamics during the condensation and increase the water collection efficiency. The surface wettability is strictly related to the surface energy and can be principally controlled via two factors, the chemical composition and the surface roughness [4]. Hydrophilic surfaces favour the nucleation of droplets but can lead to the formation of a liquid film on the cooled surface as the condensation proceeds, negatively affecting both the heat transfer and the water collection mechanism. Hydrophobic substrates, on the contrary, are characterized by the formation of isolated liquid droplets and their subsequent roll-off from the surfaces, allowing efficient water collection and favouring the renewal of the surface for cyclic condensation and droplet removal. The surface morphology is capable of enhancing both the hydrophilic and the hydrophobic properties of a substrate, as evidenced by the Young's equation [5].

Combining surface functionalization and nano-micro structuring has been widely investigated, from superhydrophobic surfaces to hybrid surfaces with mixed hydrophilic-hydrophobic wettability [6–9]. Generally, nano or micropatterning of surfaces has been employed to enhance the efficiency in a wide range of applications, including memory devices, microfluidics, cell-culture systems, heat exchangers and water-collectors [10–13]. Regarding the last two applications, the successful control of the condensation dynamics in a dropwise manner in heat exchangers can lead to an enhancement of the heat transfer coefficients of one order of magnitude compared to filmwise condensation, and to a substantial increase of the water harvesting efficiencies in related devices [4, 9, 14]. The daily phenomena of humid air condensation involving external surfaces can be manipulated with the aid of patterned films, to gain a precise control of the quantity of water collected and heat exchanged.

Considering the already existing solutions in nature, our group has previously developed a hybrid patterned coating, inspired by the exoskeleton of a Namib desert beetle [15]. The back of the beetle is covered with hydrophilic bumps that favour humid air condensation in harsh environments, while the hydrophobic wax surrounding the bumps allows the droplets to detach and roll-off into the beetle's mouth. Taking inspiration from the beetle, in our previous work a hydrophobic organic-modified silica coating with hydrophilic bumps was developed via a sol–gel process, and the dewetting mechanism was exploited to gain the patterned morphology. The sol–gel method was chosen due to the lower costs and facile control of the synthesis with respect to other vacuum-based processes, together with the chemical inertness and higher resistance provided by the inorganic components with respect to polymer-based coatings.

Regarding the dewetting mechanism, extensive research is available in the literature when polymers are considered [16–19], but only a few researchers [20] address the dewetting of sol–gel inorganic materials. The *dewetting* involves the spontaneous breakage of an unstable liquid coating on the surface of a non-wetting substrate, determined by the difference in their surface tensions [15, 17].

In our preliminary work [15], the beetle's patterned morphology was reproduced by initially spin coating a plain sol–gel silica film on a hydrophobic CH_3-silica layer, which was previously deposited on a monocrystalline silicon wafer. The increased hydrophobicity of the bottom layer with respect to the top silica film was enabled by the introduction of organic $-CH_3$ group inside the inorganic silica network [21]. The instability of the hydrophilic top-layer was induced by enclosing it in a solvent-saturated atmosphere, causing the already labile bonds to break apart due to Rayleigh instability leading to the formation of growing holes. This was possible due to the permeability of the freshly spun xerogel to the solvent vapours, since the latter holds an active role in the condensation reactions during the sol–gel process [15]. After several seconds, the originally uniform film was transformed into isolated droplets, which autonomously distributed themselves following the Voronoi geometry [16, 19]. To find the most controllable and reproducible morphology, the influence of different parameters was considered during the

optimization steps on silicon wafers, namely the aging time of the solution, the concentration, and the environmental conditions during the deposition.

Starting from these preliminary studies [15], in this work we investigated the influence of a different substrate on the reproducibility of the sol–gel dewetting. A change in the substrate results in a variation in its surface tension and morphological properties, and therefore to a variation in the forces exerted on the above unstable coating. To verify the reliability of the pattern's application in real environments, the hybrid coating was deposited and optimized on metallic aluminium surfaces with larger dimensions with respect to the silicon substrates used in our previous study, confirming the possibility of tuning the size and the distribution density of the hydrophilic bumps.

Since the literature recently evidenced the possible degradation of silica-based films after interaction with saturated water vapour [22–24], the coatings' resistance was tested under static environmental conditions of high relative humidity. In our previous studies, several hybrid organic-inorganic sol–gel coatings were employed to induce a dropwise condensation during the saturated vapour condensation, which led to an enhancement of the heat exchanged during the process [25, 26]. Here, the influence of the morphology was additionally considered, besides the variation of the chemical composition provided by the presence of a coating on the substrate. The possibility offered by the patterned morphology to enhance the drainage rate during condensation from humid air was assessed in a custom-made apparatus, by comparing the efficiency in terms of condensed mass with a bare aluminium substrate and with a plain hydrophobic CH_3-silica coating.

2 Experimental details

2.1 Materials

All materials employed were used as received, except if otherwise stated: TEOS (98%; Sigma Aldrich), MTES (98%; Sigma Aldrich), absolute ethanol (EtOH, Emsure; Sigma-Aldrich). Dilute hydrochloric acid (1 M) was obtained from concentrated hydrochloric acid (HCl, 37%; Sigma Aldrich) and milliQ water (18.2 MΩ). The metallic substrates used were made of aluminium with high purity (AW1050, 99.50% minimum aluminium content). The dimensions of the square aluminium substrates were 20×20 mm^2 in the case of the static tests and 40×40 mm^2 for the humid air condensation tests, respectively. The side exposed to the condensation phenomenon was polished following a standard metallographic technique to obtain a smooth mirror-like surface.

2.2 Preparation of the patterned coatings and the plain films

The coatings were synthesized following the procedure described by Colusso et al. [15]. The patterned coatings were developed starting from a sol–gel bilayer. To synthesize the bottom CH_3-silica layer, an acid-catalyzed solution was prepared by mixing tetraethylorthosilicate (TEOS), methyltriethoxysilane (MTES), ethanol (EtOH), 1 M hydrochloric acid (HCl) and water (H_2O) for 1 h at 400 rpm at room temperature, in molar ratios of (TEOS + MTES):EtOH:H_2O:HCl = 1:2:4:0.01, respectively, with a TEOS:MTES molar ratio of 1. After the first 30 min of mixing, additional solvent was added to reach a theoretical final concentration of SiO_2 of 1.3 M. Following the first hour of stirring, the solution was aged for 30 min, filtered with syringe filters with 0.2 µm pores and deposited on the polished aluminium substrates, which were previously cleaned through sonication in EtOH followed by atmospheric plasma cleaning (Plasma Cleaner, PDC-002-CE, Harrick Plasma). The deposition was done by spin coating at 2000 rpm for 30 s, after which the film was aged at room temperature for 24 h to allow a gradual solvent evaporation and a proper evolution of the condensation reactions and then annealed at 200 °C for 4 h. The top hydrophilic silica layer was synthesized following an analogous acid-catalyzed sol–gel process. The solution was prepared by mixing EtOH:TEOS:H_2O:HCl in a molar ratio of 2:1:4:0.01, respectively, which was stirred for 30 min and diluted with the solvent to gain a final theoretical concentration of silica between 0.75 M and 2 M. After 24 h of aging, the solution was filtered (0.2 µm pore size) and deposited on the bottom hydrophobic layer. To induce the dewetting, the as-deposited unstable film was exposed to a solvent-saturated atmosphere by enclosing the bilayered sample inside a closed cell. The destabilization of the upper film determined the formation of growing holes, which eventually allowed the evolution of the film into isolated droplets. The as-created patterned coatings were aged at room temperature for 24 h and annealed at 200 °C for 2 h. For comparison, plain CH_3-silica and silica coatings were prepared according to the same protocol.

2.3 Characterizations

The thickness of the plain films was measured with a J.A. Woollam Co. spectroscopic ellipsometer (Woollam M2000) at incident angles of 65–70–75° in a 300–1200 nm range. The materials were modelled by using Cauchy models and the final values were obtained from the average of three characterizations, measured at three distinct points on the same sample.

The chemical bonds were characterized via Fourier-transform infra-red spectroscopy (Jasco FTIR 4200), in the 4500–400 cm^{-1} at 64 scans min^{-1} and with a 2 cm^{-1}

resolution. The absorption spectra were obtained in attenuated total reflectance (ATR) mode by using air as the reference.

An atomic force microscope (AFM—Park Systems XE-70) was used to characterize the surface roughness of the plain coatings.

Optical micrographs of the samples were collected with a Leica DMRE optical microscope. Surface morphology of the samples was investigated by scanning electron microscopy (FE-SEM, Zeiss).

The dynamic contact angles were measured with the aid of a goniometer and an addition-removal method, by dispersing and subsequently withdrawing a water droplet of approximately 5 μL volume. The measurements were conducted with a home-made set-up consisting of a DCC1545M CMOS sensor camera (Thorlabs GmbH®, Bergkirchen, Germany) and MVL7000 sensor lens (Thorlabs GmbH®, Bergkirchen, Germany).

2.4 Resistance to conditions of high relative humidity

The patterned coatings and the plain CH_3-silica films, deposited on the smaller square substrates, were enclosed inside a home-made humidity test chamber for increasing exposure times of 1 day, 14 days and 30 days, respectively. The chamber consisted of a sealed glass vessel and the humidity was controlled by a saturated salt solution (potassium nitrate, 94–96% RH, 20–25 °C) [27]. The RH was monitored by a commercial sensor (Bel-Art, Scienceware digital hygrometer). Three samples for each type of coating were tested.

2.5 Condensation tests

The square aluminium substrates described in Section 2.1 were placed in a wind tunnel developed for the study of condensation from humid air over vertical metallic surfaces. After the conditioning stage, the air enters the wind tunnel and it flows over the aluminium surface ($A = 16$ cm^2), where a fraction of the water vapour present in the airflow is condensed. The condensate water is collected in a receiver that is weighed continuously by a high precision balance. Condensation tests were performed at constant air conditions (temperature of 28 °C, relative humidity of 50%, and velocity of 1 m s^{-1}), while the dew-to-wall temperature difference (ΔT) was varied in the range 4–10 K by controlling the air-cooled Peltier device connected to the substrate. The tests start with the condensing surface dry. After the air inside the wind tunnel has reached steady-state conditions, the Peltier element is activated to lower the temperature of the substrate. At this point, all experimental data, in particular the mass of the condensate produced, are recorded for 90 min. Each experimental data set is given as the average of 30 measurements recorded over 1 min with error bars representing the combined uncertainty, calculated considering the "Type A" and "Type B" components as described in the ISO Guide [28].

3 Results and discussion

3.1 Synthesis and characterization of the patterned, silica and CH_3-silica coatings on aluminium substrates

3.1.1 Synthesis of the sol–gel coatings: plain silica, plain CH_3-silica and patterned coating

The influence of the patterned coating on the condensation dynamic was evaluated by comparing it to a bare polished aluminium substrate. The patterned morphology was derived from the dewetting of a hydrophilic upper coating on a hydrophobic bottom layer, which was previously deposited on the metallic substrate. For the bottom hydrophobic layer, an initial colloidal solution was prepared by mixing TEOS and MTES precursors in an equimolar ratio, aged to favour the correct evolution of the condensation reactions and spin-coated on the precleaned aluminium substrates (see Section 2.2 for the detailed synthesis description). After 24 h of drying in air to favour a gradual solvent evaporation, the films were annealed at 200 °C to consolidate the film while avoiding thermal degradation of the organic groups. The elimination of the latter would compromise the hydrophobicity of the coating, leading to an increase of the coating wettability. Following the deposition of the hydrophobic bottom layer, the upper hydrophilic silica layer was synthesized and deposited with an analogous method. Several silica concentrations of the solution were tested to analyze the influence on the dewetted droplets morphology. The dewetting was induced by spin coating the TEOS-based solution on the non-wetting bottom layer and rapidly enclosing the freshly spun film inside a closed cell, in which the solvent-saturated atmosphere led to the destabilization of the gel chains and the gradual formation of droplets due to the growing holes. The isolated droplets obtained were aged for one day and subsequently annealed to improve their stability and densification while simultaneously avoiding thermal and mechanical stresses.

To extend the comprehension and control of the dewetting mechanism and to gain a deeper knowledge on how different morphologies and chemical compositions influence the condensation from humid air, plain silica and plain CH_3-silica coatings were also deposited on the aluminium substrates. The plain CH_3-silica coating was synthesized and deposited following the same procedure as described for the bottom layer of the patterned coating. Regarding the plain silica films, the synthesis described for the top-layer in the pattern was identically reproduced, but after the deposition by spin coating, the silica films of different

concentrations were aged for one day and then annealed in a furnace for their densification and stabilization.

3.1.2 Characterization of the plain silica and the plain CH_3-silica coatings

The changed wettability of the coated surfaces compared to the bare aluminium sample was verified by measuring the dynamic contact angles and detecting the appearance of the characteristic FTIR peaks. The advancing (ACA) and receding contact angles (RCA) of the CH_3-silica coating were 89° ± 3° and 72° ± 2°, respectively, while the bare aluminium contact angles were 65° ± 3° and 10° ± 3°. The corresponding values for the plain silica coatings were 58 ± 3° and 45° ± 2°. The generally accepted definition considers a surface to be hydrophobic if the static contact angle is above 90°, but no general agreement can yet be found in the literature on how to consider the influence of the dynamic evolution of a droplet on a surface. In the present case, indeed, the general definition would lead to defining both the surfaces as hydrophilic, but a favoured droplet removal from the surface is only allowed by the plain CH_3-silica-coated sample and impeded on the bare aluminium. Recently, several authors [4, 9] have started to describe the overall phenomenon during the droplet-substrate interaction with the aid of dynamic contact angles, among which the difference between the ACA and RCA, or hysteresis, provides an estimation of how easily the droplet can be removed from the surface. Regarding the present surfaces, the bare aluminium sample was characterized by a high hysteresis of the contact angle of 55° ± 3°, which is considerably higher than those of the coated samples, namely 17° ± 3° for the plain CH_3-silica film and 20° ± 3° for the plain silica. Considering the recent literature and the droplet evolution during its deposition and removal from the surface, in the present paper the CH_3-silica coating was classified as hydrophobic, while the bare aluminium was defined as hydrophilic. The successful introduction of the organic methyl group inside the silica network of the CH_3-silica coating was verified with the aid of FTIR. As reported in Fig. S1a, the presence of the characteristic CH_3-Si bond is visible through the 1250 cm^{-1} peak, together with the C–H bond vibration of CH_3 at 2970 cm^{-1}. All the sol–gel coatings showed the typical silica peaks at 1150–1070, 790 and 450 cm^{-1}, which correspond, respectively, to the longitudinal-transversal optical components of the Si–O antisymmetric stretching, the Si–O symmetric stretching and the Si–O–Si rocking vibrations. The 930 cm^{-1} peak indicates the presence of the O–H stretching vibrations of the unreacted Si–OH or Si–O^- groups, while the wide band at 3600–3000 cm^{-1} arises from the water adsorption which also leads to Si–OH bonds [21]. When compared to the plain silica coating, (Fig. S1b), the –OH and H_2O vibrations of the CH_3-silica coating at 3600–3000 cm^{-1} decrease in intensity with respect to the stronger vibrations detectable for the plain silica film. The weaker intensity of bands associated with the adsorbed water constitutes an additional confirmation of the presence of the methyl group inside the silica network, since the presence of such organic groups increases the hydrophobicity of a coating while reducing the quantity of adsorbed water [21, 29].

3.2 Optimization and environmental resistance of the patterned coatings on aluminium substrates

3.2.1 Optimization of the patterned morphology

Considering that the condensation mode and dynamics can be greatly influenced by the morphological and chemical properties of the condensing surface [22, 30], our previous paper [15] was centred on the synthesis and optimization of different morphologies obtained by exploiting the dewetting process on silicon wafers. To verify the patterned coating's reproducibility on substrates for real applications, in the current article the concentration of the TEOS-based solution was varied for studying the dewetting process on aluminium substrates. In the sol–gel process, the sol concentration is directly related to the thickness of the resulting thin film and therefore to the morphology of the dewetted droplets. The silica concentration of the initial colloidal solution was varied from 0.75 M to 2.0 M, which led to the corresponding patterns reported in Fig. 1.

The dewetting process was successfully reproduced and scaled on substrates with larger dimensions with respect to the previously studied silicon wafers. Consistent with the latter, the linearity of the correlation between the concentration or thickness with the mean diameter was confirmed for the aluminium substrates, as well as the correlation with the particle density (Fig. 2).

The increasing concentration of the precursor solution led to an increase in the plain silica films' thickness and therefore to bigger mean diameters and lower particle densities. The mean diameter of the particles varied from 26 ± 1 to 52 ± 7 μm when the concentration increased from 0.75 to 1.5 M, which simultaneously led to a variation of the particle density from 53 ± 5 to 11 ± 2 mm^{-2}. Analogously to the previously obtained patterns on the silicon wafers [15], the existence of a lower limit in the tunability range was confirmed for the aluminium substrates. At concentrations below 0.75 M, the dewetting of the film occurred during the deposition step by spin coating and could not be controlled via exposure to the solvent-saturated atmosphere. The higher value of the lower concentration limit resulted in a decrease in the tunability range of the droplets' sizes on aluminium with respect to that previously obtained for the silicon wafers. On the latter, the diameters could be varied by one order of magnitude (7 ± 1–59 ± 12 μm range) between 0.3 and

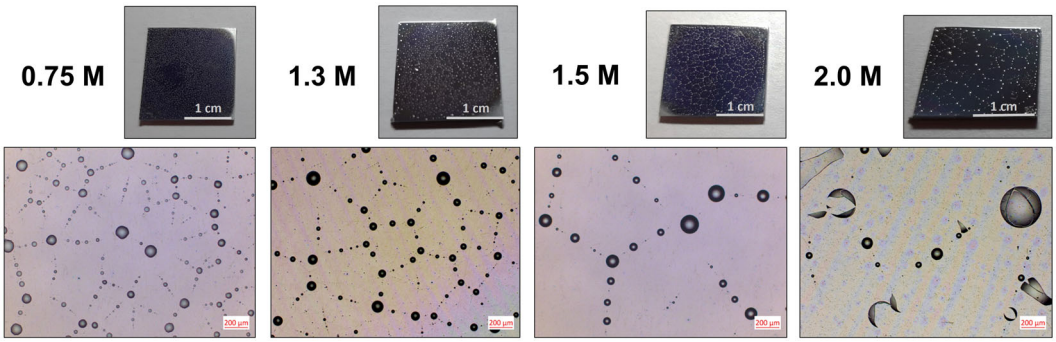

Fig. 1 Photographs and optical micrographs of patterned films on aluminium for top silica layers produced from sols with different concentrations. At 2.0 M cracks begin to form

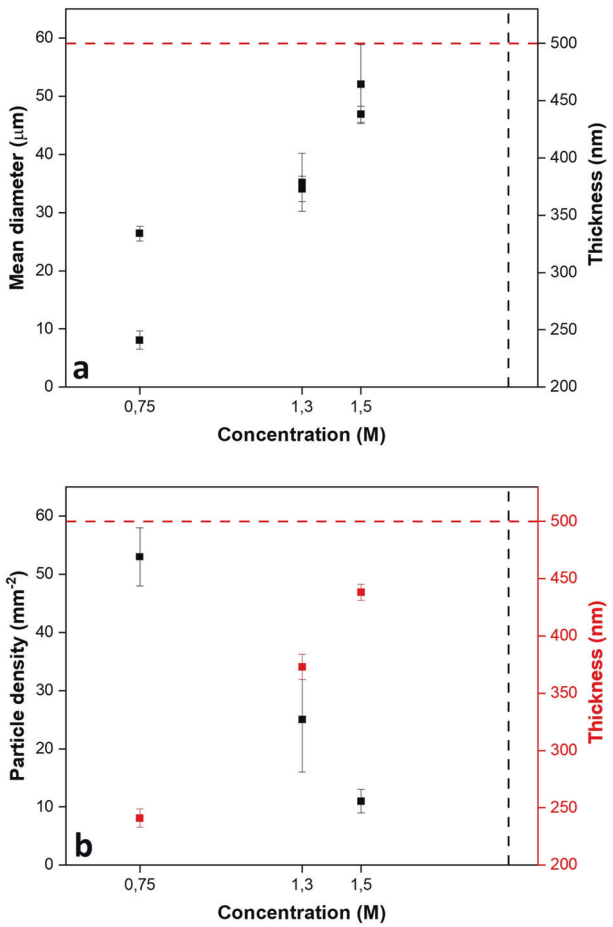

Fig. 2 Correlation between (**a**) mean diameter, (**b**) particle density of each pattern with the corresponding concentration and thickness of the top silica layer. The dotted lines indicate the concentration and thickness limit above which the silica layers crack after the thermal treatment. Each value derives from the average of three different measurements with the standard deviation

1.3 M [15]. For 0.75 M concentration, nearly the same particles' diameter was found on both aluminium and silicon, despite the film's thickness being almost twice as great on aluminium (241 ± 8 nm) compared to the corresponding layer on silicon (nearly 140 nm) [15]. By increasing the concentration to 1.3 M, the initial film's thickness was similar on both substrates, but the diameter of the particles was nearly twice as high on aluminium (35 ± 5 µm) with respect to those on silicon (59 ± 12 µm). To better mimic the 500 µm hydrophilic bumps of the beetle, the concentration was further increased up to 2.0 M compared to the values considered for the previous silicon substrates. As seen in Fig. S2, the corresponding plain silica film obtained from a 2.0 M solution was subjected to

elevated stresses during the thermal treatment, which led to the formation of cracks throughout the film. Analogously, as reported in Fig. 1, the cracks' formation is detectable on the dewetted particles obtained from the 2.0 M solution. Therefore, an upper limit in the solution concentration was found, which limits further increases of the particles' mean diameter.

An explanation of the different behaviour, in terms of particle size and dimension, between the silicon wafer and the aluminium substrate can be related to the surface properties of the two substrates. The two materials are characterized by substantially different surface tensions (around 0.07 J/m^2 for silicon wafers [31] and around 0.9 J/m^2 for pure aluminium [32]) and roughness, which strongly influence their interaction with the coatings. The surface roughness of the samples was evaluated by AFM. The root-mean-square roughness (rms) of the bare aluminium surface was 6.6 ± 0.7 nm, which is one order of magnitude higher with respect to the rms of the plain silicon wafer (0.2–0.3 nm) [15]. The higher roughness of the metallic surface is caused by the mechanical polishing procedure used to reach a mirror-like quality, which cannot completely guarantee the removal of impurities and asperities from the surface. The latter determines the formation of unwanted preferential nucleation sites, which influence, together with the physical-chemical surface properties, the final morphology of the dewetted droplets and could explain the increased particle densities with respect to the silicon substrates. Globally, the reproducibility and scalability of the dewetting process were confirmed on the aluminium substrates.

3.2.2 Environmental resistance of the patterned coatings

A fundamental prerequisite regarding the use of the patterned coatings for industrial purposes is their resistance under the harsh conditions which often characterize real working applications. The recent literature evidenced the critical interaction between water molecules and silane-based films, which suffer from delamination after a prolonged exposure to water vapour [22, 33, 34]. As evidenced by Miljkovic and co-workers, the coating degradation initiates at specific pinholes present in the films, in which the osmotic pressure promotes the rupture of the Si–O–X bonds due to hydrolysis reactions [22]. Here, the coatings were preliminary tested in static conditions of elevated relative humidity (95% RH), to verify their resistance before the condensation tests were performed. As a representative sample, the patterned coating prepared from the 1.3 M solution was chosen for investigation, since the range of the sizes and distributions of the droplets on aluminium was substantially inferior to that obtained on silicon wafers. The corresponding mean diameter, particle density and percentage of the occupied surface of the patterned coatings, obtained from image analysis of the optical micrographs, are reported in Table 1.

Table 1 Particle density, mean diameter, occupied surface, advancing and receding contact angles of the as prepared sample before the condensation tests. The values derive from the average of three measurements with the standard deviation

	As prepared sample
Mean diameter (μm)	31 ± 9
Particle density (mm^{-2})	45 ± 17
Occupied surface (%)	3.4 ± 0.2
Advancing CA (°)	82 ± 1
Receding CA (°)	70 ± 2

The hydrophilic bumps have a mean diameter of 31 ± 89 μm and are distributed on the surface with a density of 45 ± 17 particles/mm^2. The ACA and RCA are 82° ± 1° and 70° ± 2°, respectively, which are similar to the values of the plain CH_3-silica coating (see Section 3.1). This can be explained by considering the percentage of surface occupied by the hydrophilic droplets on the bottom hydrophobic layer, which is only nearly 3%; therefore the hydrophilic bumps only provide a marginal contribution to the global dynamic contact angles. Moreover, the hysteresis of the contact angle of the patterned coating is similar that of the plain CH_3-silica coating, confirming that the presence of the hydrophilic bumps on the surface does not constitute an obstacle to detachment of the liquid droplets during the vapour condensation.

During the environmental resistance tests, both the plain CH_3-silica and the patterned coatings were deposited on aluminium substrates and subjected to an increasing time of exposure under conditions of high relative humidity (95% RH). The samples were tested for increasing exposure times of 1 day, 14 days and 30 days, respectively, and the degradation was evaluated in terms of variations of the dynamic contact angles, the characteristic peaks in the FTIR spectra and the morphology observed with the optical microscope. Both the patterned coating and the plain CH_3-silica film successfully proved their resistance to the high relative humidity for up to 30 days, demonstrating no variation in the dynamic contact angles (see Fig. S3). Moreover, the FTIR measurements confirmed the presence of the organic groups even after 30 days of tests (see Fig. S4).

3.3 Humid air condensation tests

The influence of the plain hydrophobic film and the patterned coating on the condensation dynamics was analyzed and the results were compared to the condensation performance on a bare aluminium sample.

The different condensation dynamics of the three samples are visible in Fig. 3. During the temporal evolution of

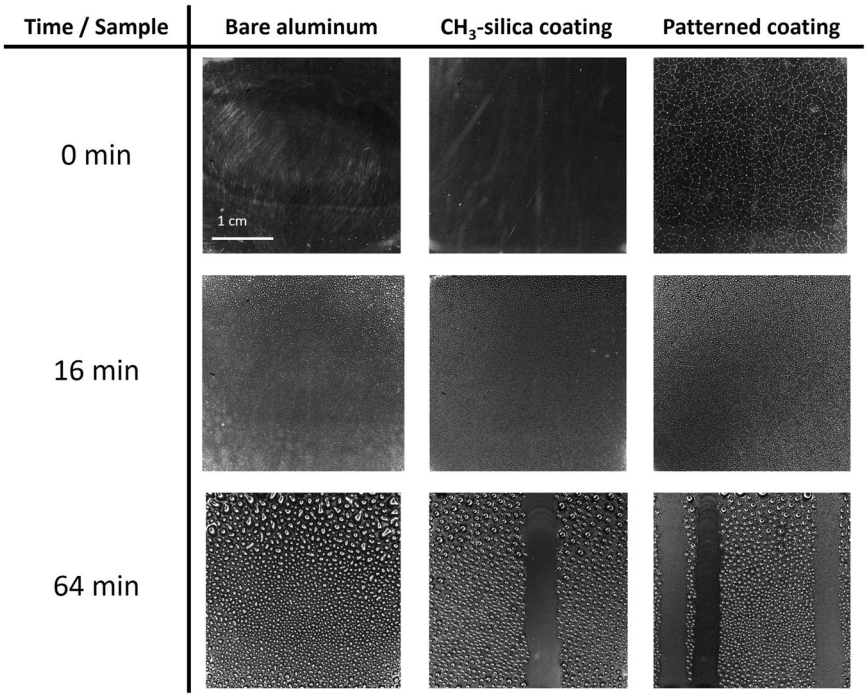

Fig. 3 Evolution of the condensation process observed on the bare aluminium, the CH_3-silica coating and the patterned coating at the same operating conditions ($\Delta T = 4$ K, $T =$ 28 °C, $v_{air} = 1$ m s^{-1} and RH = 50%)

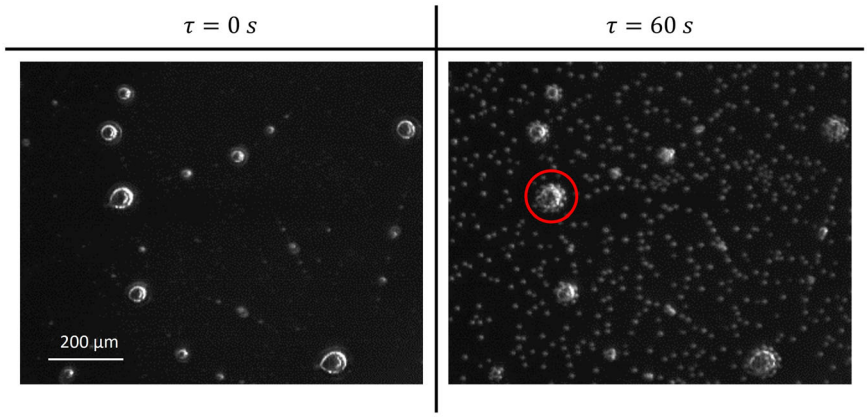

Fig. 4 Evolution of the condensation process observed on the patterned coating. The images, obtained at the same operating conditions ($T = 28$ °C, RH = 50%, $v_{air} = 1$ m s^{-1}, $\Delta T =$ 4 K), were recorded by using a high-speed camera coupled to a microscope lens (12×). Visualized area of ~ 1 mm^2. The red circle highlights a hydrophilic silica spot, on which an increased density of condensed water droplets is visible

the test, the condensate formed irregular liquid droplets on the bare aluminium surface. Due to the hydrophilicity of such substrates, the droplets exhibited a substantial adhesion to the surface and a flat irregular morphology. The elevated affinity and superficial contact of the liquid droplets with the bare aluminium resulted in their gradual aggregation into non-uniform, large droplets. On the contrary, the presence of a hydrophobic coating promoted dropwise condensation on the two coated substrates, with the formation of spherical-shaped isolated droplets. The increased hydrophobicity favoured detachment of the liquid droplets from the sample and the renewal of the underlying surface, which did not occur on the bare aluminium due to the subsequent aggregation of the droplets (see Fig. 3, 64 min).

During the first moments of the interaction between a surface and water vapour, it is known that the nucleation of the droplets is enhanced on hydrophilic surfaces compared to hydrophobic ones [8, 9]. After 60 s, it can be seen in Fig. 4 that the density of the small condensed droplets is considerably higher on the hydrophilic bumps respect to the surrounding hydrophobic areas. The presence of a hybrid morphology, composed of hydrophilic spots surrounded by hydrophobic areas, allowed to enhance both the nucleation and the removal of the liquid droplets, which is not possible to obtain on surfaces characterized by a single type of wettability. The hydrophilic bumps favoured the increase in the nucleation density, but due to their small percentage with respect to the total surface area, they did not affect the condensation mode.

The condensed mass collected during the condensation of humid air was evaluated at two different subcooling conditions ($\Delta T = 4$ and 10 K), namely at increasing differences between the dew temperature and the condensing surface temperature, to reproduce distinct industrial working conditions. The condensation performance was analyzed at increasing times of 15, 30 and 60 min. From the results reported in Fig. 5, the advantages provided by the presence of the hydrophobic coatings on the metallic surfaces were confirmed.

For each subcooling degree, the condensed mass obtainable on the bare aluminium was significantly less than that obtained in the case of both hydrophobic films. During the first 15 min at $\Delta T = 4$ K, the patterned coating and the bare aluminium substrate resulted in a 20% increase of the condensed mass with respect to the plain hydrophobic surface. This behaviour confirms the theoretical studies on the condensation dynamics, which stress that hydrophilic surfaces favour the nucleation of the liquid droplets [4]. During condensation in the presence of humid air, non-condensable gases strongly limit the overall condensation performance compared to the case of pure steam condensation [35]. Therefore, droplets nucleation and growth are slower and involve a significantly lower amount of condensed mass. Compared to the saturated vapour condensation, in the case of humid air the dynamics of the nucleation and growth are slower and involve a significantly smaller amount of condensed mass. As shown in Fig. 3, the bare aluminium substrate represents a typical hydrophilic material, which is also supported by the dynamic contact angles reported in Section 3.1. The surface of the patterned coating, despite the global hydrophobicity, is characterized by the presence of hydrophilic bumps, which favour the nucleation of the liquid droplets as seen in Fig. 4. After 15 min at $\Delta T = 10$ K the patterned coating exhibited a 24% increase of the collected mass with respect to the bare aluminium, and a 9% increase with respect to the plain hydrophobic film. By increasing the subcooling degree, the driving force for the mass transfer mechanism increases and the condensation of the water vapour in humid air is favoured, explaining the higher values of the condensed mass. With increasing interaction time between the humid air and the condensing surfaces at 30 min and subsequently at 60 min, the condensation performance of the patterned surface started to be comparable to the plain CH_3-silica coating (Fig. 3). The similar efficiencies promoted by the plain and the patterned coatings can be explained by considering the weak wettability contrast in the pattern. The difference in wettability between the hydrophilic drops and the surrounding hydrophobic areas may be not sufficient to induce evident enhancements of the collected mass. Moreover, since the hysteresis of the contact angle was recently found to be a fundamental factor for the control of the condensation dynamics [36], besides the static contact angle, the similar values of both the parameters for the two samples, can also provide an explanation of the similar efficiencies of the two hydrophobic coatings. As confirmed by the literature [30], the formulation of a hybrid wettability surface requires careful optimization of both the morphology of the surface and the degree of the wettability contrast between the highly hydrophilic areas and the highly hydrophobic ones. Moreover, the optimized parameters of morphology and wettability may change as a function of the humid air conditions. In our previous paper, the patterned coating on the silicon substrate enabled the maximum performance to be reached at very low degrees of subcooling (70% RH, $\Delta T_{d\text{-}w} =$ 3.3 °C) [15], which represent the typical conditions found in arid environments. By changing the type of substrate, the different interactions with the coating led to a variation of the patterned morphology, namely of the particle size and distribution density, and therefore to a change in the condensation performance. Nonetheless, the enhancement of the condensed mass provided by the presence of a hydrophobic coating on the metallic surface was confirmed also at increasing times of 30 and 60 min, together with the opportunity to control the condensation dynamics.

Following the humid air condensation tests, both the patterned coating and the plain hydrophobic films were characterized to verify any variation of their chemical and physical properties. Considering the dynamic contact angles (Fig. 6a), the unchanged value of the ACA confirmed the presence of the $–CH_3$ organic groups within the hybrid silica network after the condensation tests. A slight decrease of the RCA was found after the condensation tests for both the hydrophobic samples. Further confirmation of the presence at 1250 cm^{-1} of the characteristic peak of the organic groups, which are responsible for the hydrophobicity of the coatings, was provided by the FTIR spectra (Fig. S5). The ellipsometry measurements on the plain CH_3-silica film confirmed that the thickness did not vary after the condensation tests (Table S1), while the integrity of the coatings' surface was verified by SEM analysis (Fig. 6b), with no cracks nor degradation evident after exposure to the high relative humidity environment. Therefore, the resistance to humid air condensation was verified for both the hydrophobic coatings.

4 Conclusions

We reported the successful scalability and reproducibility of the dewetting process of silica-based sol–gel bilayers on metallic substrates. The diameter and the distribution density of the dewetted droplets was controlled and tuned between nearly 26–52 μm and 53–11 particles/mm^2, respectively. To verify the feasibility for industrial applications, the influence of the patterned morphology during condensation from humid air was assessed in terms of condensed mass in a custom-made

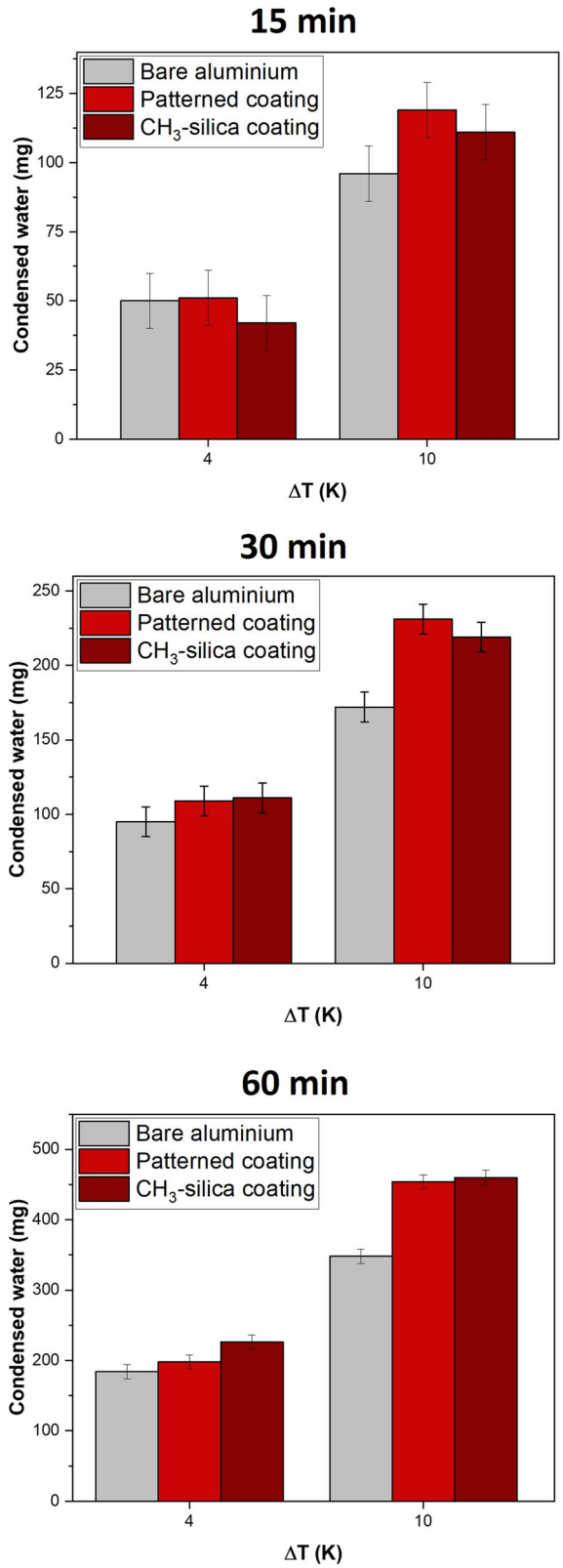

Fig. 5 Condensed mass as a function of the subcooling degree of the bare aluminium, the patterned coating and the plain CH_3-silica coating, at the same operating conditions ($T = 28$ °C, RH = 50%, $v_{air} = 1$ m s^{-1}, $\Delta T = 4$–10 K). The error bars represent the experimental uncertainties calculated as described in Section 2.5

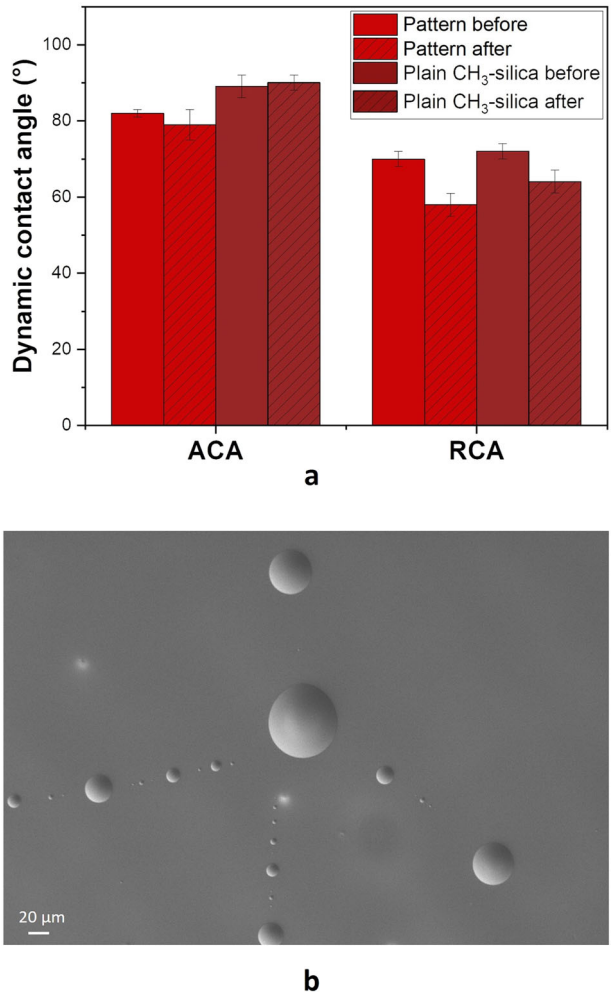

Fig. 6 **a** Dynamic contact angles of the patterned coating and the plain CH_3-silica film, before and after the humid air condensation tests. Each value derives from the average of three different measurements with the standard deviation. **b** SEM images of the coated sample, after the humid air condensation

apparatus. During the first 15 min of the condensation tests at 50% RH and $\Delta T = 4$–10 K, the hydrophilic bumps of the pattern favoured the formation of droplets compared to the surrounding hydrophobic areas. With respect to the bare aluminium, the patterned coating at a subcooling of 4–10 K enhanced the condensation performance by 21–24%, confirming the crucial role of the coatings in the control of the condensation dynamics.

Future effort will be devoted to the investigation of different geometries and wettability contrasts of the pattern, to evaluate their influence on the condensation dynamics of the humid air.

Acknowledgements We acknowledge the financial support of the Department of Industrial Engineering of Padova university through the SID 2021 project.

Funding Open access funding provided by Università degli Studi di Padova within the CRUI-CARE Agreement.

Compliance with ethical standards

Conflict of interest The authors declare no competing interests.

Publisher's note Springer Nature remains neutral with regard to jurisdictional claims in published maps and institutional affiliations.

References

1. FAO (2020). The state of food and agriculture 2020. Overcoming water challenges in Agriculture. Rome. https://doi.org/10.4060/cb1447en.
2. Jonhson W et al. (2021) Fabrication of 3D-printed ceramic structures for portable solar desalination devices. ACS Appl Mater Interfaces 13:23220–23229
3. Yarlagadda S, Gude VG, Camacho LM, Pinappu S, Deng S (2011) Potable water recovery from As, U, and F contaminated ground waters by direct contact membrane distillation process. J Hazard Mater 192:1388–1394
4. Rose JW (2002) Dropwise condensation theory and experiment: a review. Proc Inst Mech Eng Part A J Power Energy 216:115–128
5. Wen R, Ma X, Lee YC, Yang R (2018) Liquid-vapor phase-change heat transfer on functionalized nanowired surfaces and beyond. Joule 2:2307–2347
6. Yang KS, Lin KH, Tu CW, He YZ, Wang CC (2017) Experimental investigation of moist air condensation on hydrophilic, hydrophobic, superhydrophilic, and hybrid hydrophobic-hydrophilic surfaces. Int J Heat Mass Transf 115:1032–1041
7. Park KC et al. (2016) Condensation on slippery asymmetric bumps. Nature 531:78–82
8. Durán IR, Laroche G (2019) Water drop-surface interactions as the basis for the design of anti-fogging surfaces: Theory, practice, and applications trends. Adv Colloid Interface Sci 263:68–94
9. Miljkovic N, Enright R, Wang EN (2012) Effect of droplet morphology on growth dynamics and heat transfer during condensation on superhydrophobic nanostructured surfaces. ACS Nano 6:1776–1785
10. Pan T, Wang W (2011) From cleanroom to desktop: emerging micro-nanofabrication technology for biomedical applications. Ann Biomed Eng 39:600–620
11. Kim SH, Lee SY, Yang SM, Yi GR (2011) Self-assembled colloidal structures for photonics. NPG Asia Mater 3:25–33
12. He F et al. (2014) Femtosecond laser fabrication of monolithically integrated microfluidic sensors in glass. Sensors 14:19402–19440
13. Lei Y, Yang S, Wu M, Wilde G (2011) Surface patterning using templates: concept, properties and device applications. Chem Soc Rev 40:1247–1258
14. Hou Y, Yu M, Chen X, Wang Z, Yao S (2015) Recurrent filmwise and dropwise condensation on a beetle mimetic surface. ACS Nano 9:71–81
15. Colusso E, Martucci A, Neto C (2019) Fabrication of biomimetic micropatterned surfaces by sol–gel dewetting. Adv Mater Interfaces 6:1–11
16. Zhao J et al. (2004) Effects of molecular weight, solvent and substrate on the dewetting morphology of polystyrene films. Appl Surf Sci 236:131–140
17. Telford AM, Thickett SC, Neto C (2017) Functional patterned coatings by thin polymer film dewetting. J Colloid Interface Sci 507:453–469
18. Thickett SC, Neto C, Harris AT (2011) Biomimetic surface coatings for atmospheric water capture prepared by dewetting of polymer films. Adv Mater 23:3718–3722
19. Al-Khayat O, Hong JK, Geraghty K, Neto C (2016) 'The Good, the Bad, and the Slippery': a tale of three solvents in polymer film dewetting. Macromolecules 49:6590–6598
20. Kwon SJ, Park JG (2006) Dewetting of a sol-gel-derived thin film. Langmuir 22:3895–3898
21. Innocenzi P, Abdirashid MO, Guglielmi M (1994) Structure and properties of sol-gel coatings from methyltriethoxysilane and tetraethoxysilane. J Sol-Gel Sci Technol 3:47–55
22. Khodakarami S, Zhao H, Rabbi KF, Miljkovic N (2021) Scalable corrosion-resistant coatings for thermal applications. ACS Appl Mater Interfaces 13:4519–4534
23. Ma J, Cha H, Kim MK, Cahill DG, Miljkovic N (2019) Condensation induced delamination of nanoscale hydrophobic films. Adv Funct Mater 29:1–10
24. Parin R et al. (2020) Heat transfer and droplet population during dropwise condensation on durable coatings. Appl Therm Eng 179:115718
25. Parin R et al. (2018) Nano-structured aluminum surfaces for dropwise condensation. Surf Coat Technol 348:1–12
26. Parin R, Del Col D, Bortolin S, Martucci A (2016) Dropwise condensation over superhydrophobic aluminium surfaces. J Phys Confer Ser 745.
27. Greenspan L (1977) Humidity Fixed Points of Binary Saturated Aqueous Solutions. J. Res. Natl. Bur. Stand—A. Phys Chem, 81A:89–96
28. Joint Committee for Guides in Metrology (2008) Evaluation of measurement data—guide to the expression of uncertainty in measurement.
29. Yang J, Chen J, Song J (2009) Studies of the surface wettability and hydrothermal stability of methyl-modified silica films by FT-IR and Raman spectra. Vib Spectrosc 50:178–184
30. Ghosh A, Beaini S, Zhang BJ, Ganguly R, Megaridis CM (2014) Enhancing dropwise condensation through bioinspired wettability patterning. Langmuir 30:13103–13115
31. Pasquariello D, Lindeberg M, Hedlund C, Hjort K (2000) Surface energy as a function of self-bias voltage in oxygen plasma wafer bonding. Sens Actuators A Phys 82:239–244
32. Bainbridge IF, Taylor JA (2013) The surface tension of pure aluminum and aluminum alloys. Metall Mater Trans A Phys Metall Mater Sci 44:3901–3909
33. Dalmoro V et al. (2015) Improving the corrosion performance of hybrid sol-gel matrix by modification with phosphonic acid. Prog Org Coat 80:49–58
34. Juan-Díaz MJ et al. (2014) Study of the degradation of hybrid sol-gel coatings in aqueous medium. Prog Org Coat 77:1799–1806
35. Huang J, Zhang J, Wang L (2015) Review of vapor condensation heat and mass transfer in the presence of non-condensable gas. Appl Therm Eng 89:469–484
36. Kaneko S, Urata C, Sato T, Hönes R, Hozumi A (2019) Smooth and transparent films showing paradoxical surface properties: the lower the static contact angle, the better the water sliding performance. Langmuir 35:6822–6829